Appendix A: Photodissociation and photoionization cross sections

Photodissociation and photoionization processes are treated using the relevant cross section as a function of wavelength. We adopt this approach for key species for which cross section data are available in the literature, excluding H_2 and CO, the photodissociation of which are treated solving the excitation and line-by-line radiative transfer and taking into account self-shielding effects. We are mainly interested in cross sections ranging from the Lyman cutoff, at 911.776 Å, to wavelengths in the range 1500-4000 Å, where most molecules have their photodissociation threshold. We note that in protoplanetary disks, stellar photons with wavelengths shorter than the Lyman cutoff may also have an impact on the photodissociation and photoionization rates in disk regions exposed to the star. It will be worth to take into account this in the future.

Cross sections of molecules with a closed electronic shell have been mostly taken from experimental studies carried out at room temperature. In the case of radicals, most of the cross section data comes from theoretical studies. We note that cross sections can show a great dependence with temperature, something that may have an important impact on the chemistry of protoplanetary disks taking into account that the gas kinetic temperature can take values from hundreds to thousands of degrees Kelvin in the photon-dominated region of the disk. Of course it would be desirable to use temperature-dependent cross sections, although such data is currently limited to just a few species (e.g., Venot et al. 2013; McMillan et al. 2016). This will be something to take into account in the future.

We have compiled photo cross sections for 29 molecules and 8 atoms from original sources in the literature or from databases such as the *MPI-Mainz UV/VIS Spectral Atlas of Gaseous Molecules of Atmospheric Interest*[14], which contains extensive information on experimental cross sections of stable molecules, the *Photo Rate Coefficient Database*[15] (Huebner et al. 1992), the *Leiden database of photodissociation and photoionization of astrophysically relevant molecules*[16] (van Dishoeck et al. 2006; Heays et al. 2017), which contains theoretical data of numerous radicals. It is common that experimental studies provide the photoabsorption cross section without disentangling whether the absorption leads to fluorescence, dissociation, or ionization. Unless otherwise stated, we have assumed that absorption of FUV photons not leading to ionization leads to dissociation of the molecule, that is, that the contribution of fluorescence to the total photoabsortion cross section is negligible. This may be a bad approximation at long wavelengths but is likely to be correct at short wavelengths, typically below 1500 Å. In the case of photoionization of atoms we have made use of databases such as TOPbase, the Opacity Project atomic database[17] (Cunto et al. 1993), to retrieve cross sections for some of the atoms. In the next subsections we detail the cross section adopted for each of the 29 molecules and 8 atoms considered. In Fig. A.1 we show the photodissociation cross section as a function of wavelength for some key molecules.

[14] http://www.uv-vis-spectral-atlas-mainz.org
[15] http://phidrates.space.swri.edu/
[16] http://home.strw.leidenuniv.nl/~ewine/photo/
[17] http://cdsweb.u-strasbg.fr/topbase/topbase.html

A.1. CH

The photodissociation cross section of methylidyne has been taken from the calculations of van Dishoeck (1987), which comprise dissociation by lines and by continuum. The photoionization cross section has been obtained from the theoretical study by Barsuhn & Nesbet (1978). The photoionization threshold of CH is 1170 Å (Huebner et al. 1992).

A.2. CH^+

The photodissociation cross section of CH^+ is taken from the theoretical calculations of Kirby et al. (1980), where we have adopted a cross section of 10 Mb[18] at the resonances lying at 1523, 1546, and 1579 Å. Photodissociation through the three excited electronic states considered by Kirby et al. (1980), $2^1\Sigma^+$, $2^1\Pi$, and $3^1\Sigma^+$, yields as products C + H^+.

A.3. CH_2

The photodissociation cross section of the methylene radical has been taken from van Dishoeck et al. (1996), whose calculations comprise dissociation by lines and by continuum radiation. Methylene has two main dissociation channels:

$$CH_2 + h\nu \rightarrow CH + H \quad (A.1)$$
$$\rightarrow C + H_2, \quad (A.2)$$

but the latter is a minor one (Kroes et al. 1997), and has therefore been neglected here. The ionization threshold of CH_2 is 1193 Å, although there are not cross section data in the literature, except for the relative data in the ionization threshold region by Litorja & Ruscic (1998).

A.4. CH_3

The UV spectra of CH_3 has been recorded in photographic plates (Herzberg 1961; Callear & Metcalfe 1976), although no quantitative measurement of the intensity was carried out. More recently, the absolute photodissociation cross section has been measured in the 2000-2400 Å region by Cameron et al. (2002) and in the band at 2164 Å by Khamaganov et al. (2007), in good agreement with previous absolute measurements: 40.1-41.2 Mb at 2136.6 Å (Macpherson et al. 1985) and 35.1 Mb at 2164 Å (Arthur 1986). We have adopted the photodissociation cross section measured by Cameron et al. (2002) and Khamaganov et al. (2007) at wavelengths longer than 2000 Å, and have calibrated the band intensities classified in five categories, from very weak to very strong, by Herzberg (1961) based on the absolute cross section measured for the 2164 Å band. The dissociation of the methyl radical has two possible channels:

$$CH_3 + h\nu \rightarrow CH_2 + H \quad (A.3)$$
$$\rightarrow CH + H_2, \quad (A.4)$$

whose quantum yields are not clear. Channel (A.3) is observed at 2163 Å by Wilson et al. (1994), at 1933 Å by North et al. (1995), and at 2125 Å by Wu et al. (2004), while channel (A.4) is observed through fluorescence of CH at $\lambda > 1050$ Å by Kassner & Stuhl (1994). In the absence of better constraints we have assumed a quantum yield of 50 % for each channel. As concerns photoionization, we adopt the absolute cross section measured by Gans et al. (2010) from the photoionization threshold

[18] 1 Mb is equal to 10^{-18} cm^2.

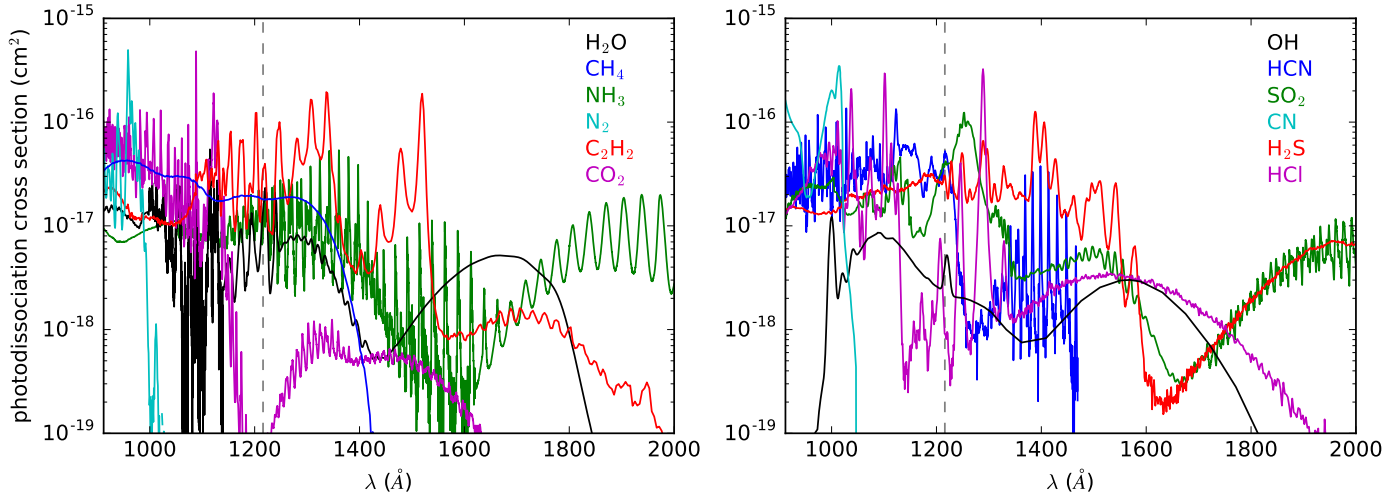

Fig. A.1. Photodissociation cross section of various molecules as a function of wavelength. The position of the Ly-α line at 1216 Å is marked with a vertical dashed line.

(1260 Å) to 1085 Å, and consider a constant cross section shortward of 1085 Å. The adopted cross section is, within uncertainties, similar to those reported in previous studies (Taatjes et al. 2008; Loison 2010).

A.5. CH_4

In the case of methane the photoabsorption cross section has been taken from the experimental study by Au et al. (1993) while the photoionization cross section (the ionization threshold of CH_4 is 983.2 Å) has been measured by Wang et al. (2008). Methane has various photodissociation channels leading to the radicals CH_3, CH_2, and CH:

$$CH_4 + h\nu \rightarrow CH_3 + H \quad (A.5)$$
$$\rightarrow CH_2(X^3B_1) + H + H \text{ or } CH_2(a^1A_1) + H_2, \quad (A.6)$$
$$\rightarrow CH + H_2 + H \text{ or } CH + H + H + H, \quad (A.7)$$

whose quantum yields have been measured by Gans et al. (2011) at 1182 Å and 1216 Å.

A.6. C_2

The photodissociation and photoionization cross sections of C_2 have been taken from the theoretical studies by Pouilly et al. (1983) and Toffoli & Lucchese (2004), respectively. The photoionization threshold of C_2 is 1020 Å (Toffoli & Lucchese 2004).

A.7. C_2H

In the case of the ethynyl radical we adopt the photodissociation cross section by lines calculated by van Hemert & van Dishoeck (2008). The main dissociation channel yields C_2 + H (Duflot et al. 1994; Sorkhabi et al. 1997; Mebel et al. 2001; Apaydin et al. 2004). The photoionization threshold of C_2H is 1068 Å (Lide 2009), although to our knowledge there are not cross section data available in the literature.

A.8. C_2H_2

For acetylene the photoionization cross section at wavelengths shorter than the ionization threshold of 1087.6 Å has been taken from the compilation by Hudson (1971). We have substracted the cross section of photoionization to the photoabsorption cross section measured by Cooper et al. (1995) to obtain the photodissociation cross section, which is assumed to yield the C_2H radical with a 100 % efficiency.

A.9. OH

The photoabsorption cross section of the hydroxyl radical has been measured by Nee & Lee (1984) in the wavelength range 1150-1830 Å. On the theoretical side, the photodissociation has also been studied by van Dishoeck & Dalgarno (1984). The experimental values are somewhat higher than the theoretical ones, although, on the other hand, calculations indicate that photodissociation by lines is also important at wavelengths shorter than 1150 Å. We adopt the theoretical photodissociation cross section, mainly because it spans over a broader wavelength range. Relative photoionization cross section has been measured by Dehmer (1984) up to the threshold at 952.5 Å (Lide 2009). The absolute scale of the photoionization cross section is fixed by setting a value of 2.5 Mb at 946 Å, according to the calculations of Stephens & McKoy (1988).

A.10. H_2O

The photoabsorption cross section of water has been taken from various experimental studies: Fillion et al. (2004) for the wavelength range 999-1139 Å, Mota et al. (2005) in the wavelength range 1148-1939 Å, and Chan et al. (1993a) elsewhere in the range from the Lyman cutoff to 2060.5 Å. The photoionization cross section for wavelengths shorter than the ionization threshold of H_2O (982.4 Å) has been taken from the experimental study of Fillion et al. (2003). Water has two main photodissociation channels, yielding OH radicals and O atoms:

$$H_2O + h\nu \rightarrow OH + H, \quad (A.8)$$
$$\rightarrow O(^3P) + H + H \text{ or } O(^1D) + H_2, \quad (A.9)$$

where channel (A.8) dominates over channel (A.9). Water can be photodissociated in the first band $\tilde{X}^1A_1 - \tilde{A}^1B_1$ at wavelengths longer than 1360 Å and in the second $\tilde{X}^1A_1 - \tilde{B}^1A_1$ and higher bands at shorter wavelengths. Quantum yields of 78 % and 22 % for channels (A.8) and (A.9) have been measured by Slanger & Black (1982) at 1216 Å (Lyα). We adopt these values for $\lambda < 1360$ Å while at longer wavelengths we take quantum yields of 99 % and 1 % (Crovisier 1989).

A.11. O_2

In the wavelength range of photoionization of molecular oxygen (up to the ionization threshold of 1027.8 Å, e.g., Huebner et al. 1992), the photoabsorption and photoionization cross sections have been taken from the experimental study of Holland et al. (1993). Up to 1750 Å the photoabsorption cross section has been taken from in the Yoshino et al. (2005), and from Chan et al. (1993b) at longer wavelengths. The dissociation threshold of O_2 is 2423.7 Å (Huebner et al. 1992), although at wavelengths longer than ∼1850 Å the photodissociation cross section already becomes negligible.

A.12. H_2CO

The photoabsorption cross section of formaldehyde is taken from the measurements by Cooper et al. (1996). The cross section of photoionization, which occurs at wavelengths shorter than ∼1400 Å, has been measured by Mentall et al. (1971). The photodissociation channels of H_2CO are

$$H_2CO + h\nu \rightarrow CO + H_2, \quad (A.10)$$
$$\rightarrow CO + H + H, \quad (A.11)$$
$$\rightarrow HCO + H, \quad (A.12)$$

where channel (A.12) can be neglected as an important one because it occurs in the wavelength range 2000-3340 Å, where the absorption cross section of H_2CO is three orders of magnitude lower than at $\lambda < 2000$ Å. On the other hand, channels (A.10) and (A.11) occur with similar quantum yields (Stief et al. 1972). However, since the implications of producing either molecular or atomic hydrogen in the photodissociation of H_2CO are small for the chemistry of protoplanetary disks, we have assumed that only channel (A.10) occurs.

A.13. CO_2

The ionization threshold of CO_2 is 900 Å and thus photoionization does not occur in our wavelength range of interest. The adopted photoabsorption cross section is based on the critical evaluation by Huestis & Berkowitz (2010). The only allowed channel in the photodissociation of carbon dioxide is that yielding CO + O (see, e.g., Huebner et al. 1992).

A.14. NH

In the case of the NH radical the photodissociation cross section has been calculated by Kirby & Goldfield (1991). The photoionization cross section has been calculated by Wang et al. (1990) to be around 8 Mb in the narrow wavelength range from the Lyman cutoff to the ionization threshold at 919.1 Å.

A.15. NH_2

The photodissociation cross section of NH_2 is taken from the theoretical calculations of Koch (1997). There are two possible dissociation channels:

$$NH_2 + h\nu \rightarrow NH + H, \quad (A.13)$$
$$\rightarrow N + H_2, \quad (A.14)$$

where only channel (A.13) is considered here, based on experimental and theoretical evidence that the major channel in the photodissociation of NH_2 leads to NH radicals (Biehl et al. 1994; Vetter et al. 1996). As concerns photoionization, we used the relative cross section measured by Gibson et al. (1985) in the wavelength range 745-1125 Å (the ionization threshold is 1130 Å) and fixed the absolute scale by assuming a guess value of 10 Mb for the cross section at 912 Å.

A.16. NH_3

The photoabsorption cross section of ammonia is taken from Edvardsson et al. (1999) up to the ionization threshold of 1231 Å, from Wu et al. (2007) in the wavelength range 1231-1440 Å, and from Chen et al. (2006a) at longer wavelengths. The data measured by Burton et al. (1993) at a lower spectral resolution is consistent with the data described above. The photoionization cross section has been taken from Edvardsson et al. (1999). As concerns photodissociation, there are different channels for ammonia, leading to NH_2 and NH radicals,

$$NH_3 + h\nu \rightarrow NH_2 + H, \quad (A.15)$$
$$\rightarrow NH(X^3\Sigma^-) + H + H \text{ or } NH(a^1\Delta) + H_2, \quad (A.16)$$

where channel (A.15) dominates over the production of NH with a yield ≥ 0.694. The quantum yields over the wavelength range of interest have been taken from various measurements carried out at different wavelengths (McNesby et al. 1962; Okabe et al. 1967; Groth et al. 1968; Lilly et al. 1973; Slanger & Black 1982).

A.17. N_2

Molecular nitrogen is ionized by photons with energies higher than 15.58 eV and thus only photodissociation, and not photoionization, occurs in our wavelength range of interest. The photoabsorption cross section has been taken from the experiments carried out by Chan et al. (1993c). The photodissociation threshold of N_2 is 1270.85 Å, although in the practice only photons with $\lambda < 1000$ Å are efficient enough in dissociating molecular nitrogen.

A.18. CN

The photodissociation cross section of the CN radical has been calculated by Lavendy et al. (1987). The photodissociation threshold is 1600 Å (Huebner et al. 1992), although in the practice the cross section becomes vanishingly small at wavelengths longer than ∼1100 Å. Since the ionization threshold of CN is 911.756 Å (Lide 2009), slightly shorter than that of hydrogen, we do not consider photoionization here.

A.19. HCN

Hydrogen is ionized by photons with wavelengths shorter than the Lyman cutoff and thus photoionization of HCN is not con-

sidered here. We have adopted the photoabsorption cross section measured by Nuth & Glicker (1982) up to λ = 1469.2 Å. We assume that at longer wavelengths the contribution to photodissociation is small and that the main photodissociation channel leads to the CN radical.

A.20. HNC

The photoabsorption cross section of HNC has been recently calculated simultaneously with that of the most stable isomer HCN by Chenel et al. (2016) in the 7-10 eV energy range. More recently, Aguado et al. (2017) have extended those calculations including higher electronic states to cover the 7-13.6 eV energy range. We adopted the cross section calculated by Aguado et al. (2017) and assumed that absorption in the studied wavelength range leads mainly to dissociation rather than fluorescence. The ionization threshold of HNC is 992 Å (Lide 2009), although the relevant cross section is not known.

A.21. NO

The photoabsorption cross section of nitric oxide was taken from Watanabe et al. (1967) up to 1350 Å and from Guest & Lee (1981) at longer wavelengths. The photoionization cross section has been measured by Watanabe et al. (1967) up to the ionization threshold, at 1340 Å. The photodissociation cross section has been obtained by substracting the cross sections due to photoionization (Watanabe et al. 1967) and to fluorescence (as characterized by Guest & Lee 1981) to the total photoabsorption cross section.

A.22. SH

In the case of the mercapto radical, various studies have investigated theoretically the photodissociation dynamics involving selected electronic states, mostly the first excited state $A^2\Sigma^+$ but also higher ones such as $^2\Sigma^-$, $^2\Delta$, and $2^2\Pi$ (e.g., Wheeler et al. 1997; Chen et al. 2006b; Janssen et al. 2007). However, no quantitative measurement of the photodissociation cross section across the FUV range is available. We have therefore adopted the photodissociation cross section from the Leiden database, whose data are largely based on the calculations of Bruna & Hirsch (1987). The photoionization threshold of SH is 1190 Å, although there are no data on the relevant cross section.

A.23. SH^+

For the SH^+ ion, the photodissociation cross section was taken from the Leiden database, where the recent calculations by McMillan et al. (2016) were used adopting the cross section of photodissociation from the ground $v = 0$ and $J = 0$ level (see Heays et al. 2017). Photodissociation at FUV wavelengths is dominated by transitions involving the excited electronic states $3^3\Sigma^-$ and $3^3\Pi$, which yield S + H^+ as products (McMillan et al. 2016).

A.24. H_2S

For hydrogen sulfide the photoabsorption cross section has been taken from Feng et al. (1999a) and the photoionization yield from Feng et al. (1999b). We just consider the dissociation channel leading to SH + H, which dominates over the others (see, e.g., Cook et al. 2001). There are two possible ionization channels (Huebner et al. 1992):

$$H_2S + h\nu \rightarrow H_2S^+ + e^-, \quad (A.17)$$

$$\rightarrow S^+ + H_2 + e^-, \quad (A.18)$$

where channel (A.17) has a threshold of 1185.25 Å and dominates, while channel (A.18) has a threshold of 927 Å and accounts for just a 5 % of the total ionization quantum yield. We therefore consider that ionization yields H_2S^+ in all cases.

A.25. CS

In the case of carbon monosulfide the photodissociation cross section was taken from the Leiden database, whose data is based on absorption lines measurements by Stark et al. (1987), vertical excitation energies calculated by Bruna et al. (1975), plus some oscillator strength guesses. For the photoionization cross section we used the relative measurements carried out by Norwood et al. (1991) in the wavelength range 1000-1100 Å (the ionization threshold is 1095.5 Å) and fixed the absolute scale by assuming a guess value of 10 Mb for the cross section at $\leq$ 1000 Å.

A.26. SO

For sulfur monoxide the cross section data available in the literature cover just a limited spectral region. The photoabsorption cross section has been measured in the wavelength ranges 1150-1350 Å and 1900-2350 Å by Nee & Lee (1986) and by Phillips (1981), respectively. In the gap between these two spectral regions and at wavelengths shorter than 1150 Å we have adopted an arbitrary photodissociation cross section of 5 Mb. The ionization threshold of SO is 1205 Å (Huebner et al. 1992). As photoionization cross section we used the photoelectron spectrum measured by Norwood & Ng (1989) in the wavelength range 1025-1225 Å and scaled it assuming a cross section of 10 Mb at $\leq$ 1025 Å.

A.27. SO_2

The photoabsorption cross section of sulfur dioxide is based on various experimental studies dealing with different wavelength ranges: Holland et al. (1995) up to the ionization threshold of SO_2 at 1004 Å, Feng et al. (1999c) in the range 1004-1061 Å, Manatt & Lane (1993) in the range 1061-1717.7 Å, and Wu et al. (2000) at longer wavelengths. The photoionization cross section is taken from Holland et al. (1995). The photodissociation of SO_2 has two possible channels:

$$SO_2 + h\nu \rightarrow SO + O, \quad (A.19)$$

$$\rightarrow S + O_2, \quad (A.20)$$

with quantum yields of 50 % for each channel, as measured by Driscoll & Warneck (1968) at 1849 Å. We adopt these quantum yields from the Lyman cutoff to the photodissociation threshold of channel (A.20), lying at 2070 Å (Huebner et al. 1992), and assume that only channel (A.19) occurs from 2070 Å to 2179 Å, this latter value being the photodissociation threshold of the channel leading to SO (Huebner et al. 1992).

A.28. HF

Hydrogen fluoride is ionized by photons with energies above 16 eV and thus only photodissociation is considered here. The pho-

todissociation cross section of HF was obtained from the theoretical calculations by Li et al. (2010), which are in good agreement with the experimental values measured in the wavelength range 1070-1450 Å by Nee et al. (1985). The photodissociation cross section of HF has the shape of a continuous band centered at ∼1230 Å, which corresponds to the $X^1\Sigma^+ - a^1\Pi$ transition.

A.29. HCl

The photoabsorption cross section of hydrogen chloride has been measured by Brion et al. (2005). The photoionization yield up to the ionization threshold of HCl, at 972.5 Å, has been taken from the study of Daviel et al. (1984).

A.30. Photoionization of atoms

We have also taken into account the photoionization cross sections of those atoms which can be ionized by photons with wavelengths longer than 911.776 Å. Among the elements included in the chemical network those atoms are, in order of increasing photoionization threshold (taken from Lide 2009 and given in parentheses): Cl (956.11 Å), C (1101.07 Å), P (1182.30 Å), S (1196.76 Å), Si (1520.97 Å), Fe (1568.9 Å), Mg (1621.51 Å), and Na (2412.58 Å). Data for chlorine have been taken from the measurements by Ruscic & Berkowitz (1983). Cross sections for sulfur and sodium were taken from the TOPbase database, while for phosphorus, carbon, and silicon we adopted the analytic fits by Verner et al. (1996)[19]. For magnesium and iron we used the cross sections in the Leiden database.

Appendix B: Photodissociation and photoionization rates

The photodissociation and photoionization rate of a given species depends on the relevant cross section and the strength and spectral shape of the FUV radiation field. In protoplanetary disks there are two main sources of FUV radiation, the interstellar radiation field (ISRF) and the star, each one having a different strength, spectral shape, and illumination geometry. Therefore, the relative contribution of each field to the various photoprocesses can be quite different depending on the particular process (via the spectral shape of the cross section) and the position in the disk (via the exposure to each radiation field).

The effect of the different spectral shapes of interstellar and stellar radiation fields on the photoprocesses occurring in protoplanetary disks has been investigated by van Dishoeck et al. (2006). These authors approximated the stellar emission of T Tauri and Herbig Ae stars as black bodies at temperatures of 4000 K and 10,000 K, respectively. One of the most dramatic effects found is that the 4000 K black body field is much less efficient in photodissociating and photoionizing molecules than the interstellar and 10,000 K black body fields. The reason is that the 4000 K black body emits little at short wavelengths, where dissociation and ionization take place. A similar study using an updated set of cross sections has been recently carried out by Heays et al. (2017). Here we have adopted as proxies of the T Tauri and Herbig Ae/Be radiation fields the spectra of TW Hya and AB Aurigae described in section 2.1.1 and shown in Fig. 1. As a consequence of the strong FUV excess and Lyα emission usually present in T Tauri stars, which is accounted for by the TW Hya spectrum but not by a blackbody at 4000 K, the photodissociation and photoionization efficiency of the T Tauri radiation field is greatly enhanced with respect to the black body assumption.

[19] http://www.pa.uky.edu/~verner/photo.html

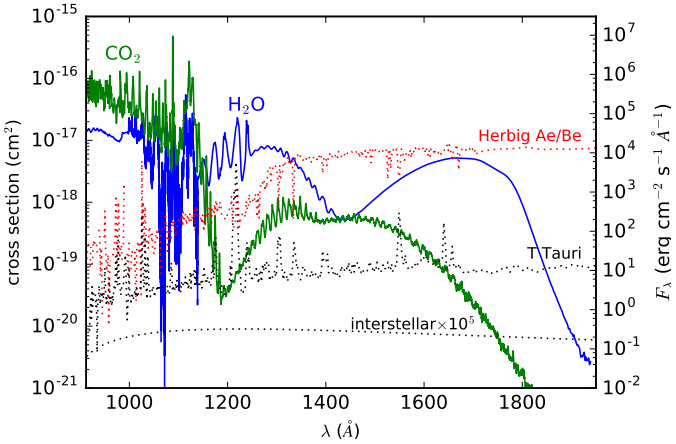

Fig. B.1. FUV photodissociation cross sections of H_2O and CO_2 superimposed on the FUV spectrum of the T Tauri and Herbig Ae/Be stars (flux at 1 au) and on the spectral shape of the interstellar radiation field. Note for example how Lyα radiation becomes very important to photodissociate H_2O but not CO_2, which is photodissociated more efficiently at wavelengths shorter than ∼1150 Å.

Following the idea of van Dishoeck et al. (2006), here we are interested in evaluating the effect of the different spectral shapes of interstellar and stellar radiation fields (see, e.g., Fig. B.1) on the photodissociation and photoionization rates of assorted species. To that purpose we have scaled the T Tauri and Herbig Ae/Be radiation fields to get the same energy density of the ISRF over the wavelength range 912-2400 Å, which amounts to 1.07×10^{-13} erg cm^{-3} adopting the ISRF of Draine (1978) and the expressions given in section 2.1.1. This is almost twice the value given by Habing (1968), 5.6×10^{-14} erg cm^{-3}. For a given radiation field characterized by a specific intensity I_λ and a photoprocess characterized by a cross section σ_λ, the rate Γ can be computed as

$$\Gamma = \int_{912}^{\lambda_{max}} \left(4\pi \frac{\lambda}{hc} I_\lambda\right) \sigma_\lambda d\lambda, \quad \text{(B.1)}$$

where the term in parentheses is the photon flux per unit time, area, and wavelength, and the integral extends from the Lyman cutoff (912 Å) to a maximum wavelength λ_{max}, which depends on each process.

In order to evaluate how the rates of the various photoprocesses vary with the depth into the disk, we have made use of the Meudon PDR code (Le Petit et al. 2006) to compute the photodissociation and photoionization rates as a function of A_V. We consider a plane-parallel cloud illuminated on one side by an external radiation field corresponding to either the ISRF, the T Tauri star, or the Herbig Ae/Be star, where the stellar fields have been scaled to the FUV energy density of the ISRF. The cloud has uniform density of H nuclei and gas kinetic temperature. We have verified that densities in the range 10^4-10^8 cm^{-3} and temperatures ranging from 100 to 1000 K, typical values in the photon dominated region of protoplanetary disks, yield identical results. The resulting photodissociation and photoionization rates as a function of the visual extinction have been fitted in the range A_V=0-5 according to the standard expression given by Eq. (7). We use this expression for simplicity, although we

note that more accurate fits can be obtained with more elaborate expressions, e.g., considering two coefficients instead of one in the exponential term (Roberge et al. 1991) or involving the 2^{nd}-order exponential integral E_2 (Neufeld et al. 2009; Roueff et al. 2014; Heays et al. 2017).

In Table B.1 we list unattenuated rates α and attenuation factors γ under different radiation fields for the photodissociation and photoionization processes involving the 29 molecules and 8 atoms discussed in Appendix A[20]. If we focus on the unattenuated rates α, we see that the rates calculated under the T Tauri radiation field are not very different from those computed under the ISRF (within one order of magnitude), while in the case of the Herbig Ae/Be radiation field some photoprocesses have rates similar to those computed under the ISRF (within one order of magnitude) while for others the rates are lower by more than a factor of ten. By looking to the spectral shape of the different FUV radiation fields (see Fig. B.1) we note that, except for the fact that stellar spectra have spectral features while the ISRF is a continuum, the spectra of the T Tauri star and the ISRF are more flat than that of the Herbig Ae/Be star, which shows a depletion of flux at short wavelengths (below ∼1300 Å). Therefore, those photoprocesses which occur more effectively at short wavelengths, as, e.g., the photodissociation of N_2 (see Fig.A.1), have higher rates under the ISRF and the T Tauri radiation field than under the Herbig Ae/Be field.

It is interesting to compare our results with previous studies. In general, the unattenuated rates α and the attenuation parameters γ calculated here under the ISRF are similar to those calculated by Roberge et al. (1991), van Dishoeck et al. (2006), and Heays et al. (2017). As concerns the rates under the Herbig Ae/Be radiation field, our parameters α and γ are also not very different from those calculated by van Dishoeck et al. (2006) and Heays et al. (2017) for a 10,000 K black body radiation field, because the FUV spectrum of AB Aurigae used by us is not drastically different from that of a 10,000 K black body. The same is not true in the case of the radiation field of the T Tauri star. The FUV spectrum of a 4000 K black body is very different from that of TW Hya, which translates into very different photodissociation and photoionization rates. In general, the rates calculated by us for a T Tauri star are orders of magnitude higher than those computed by van Dishoeck et al. (2006) and Heays et al. (2017).

The values provided in Table B.1 can be useful in chemical models of protoplananetary disks around T Tauri and Herbig Ae/Be stars, as long as they allow to compute the photodissociation and photoionization rates in a simple way, avoiding the more expensive approach, in terms of computing time, of solving the FUV radiative transfer.

[20] The interstellar unatennuated rates α in Table B.1 have been scaled up by a factor of two with respect to the output values from the one-side illuminated clouds modeled with the Meudon PDR code. This way, our tabulated values are in line with those in the literature (Roberge et al. 1991; van Dishoeck et al. 2006; Heays et al. 2017) and in the astrochemical databases UMIST and KIDA. Note, however, that when modeling protoplanetary disks or clouds that are illuminated on just one side, the other being optically thick, one must use half the unatennuated rates α listed in Table B.1.

Table B.1. Photodissociation and photoionization rates for various radiation fields.

	interstellar[a]		T Tauri[b]		Herbig Ae/Be[c]	
Reaction	α (s^{-1})	γ	α (s^{-1})	γ	α (s^{-1})	γ
CH + *hν* → C + H	9.8×10^{-10}	1.58	9.9×10^{-10}	1.02	2.5×10^{-9}	0.89
CH + *hν* → CH^+ + e^-	9.3×10^{-10}	3.20	1.6×10^{-10}	2.71	1.1×10^{-11}	2.64
CH^+ + *hν* → C + H^+	3.3×10^{-10}	3.02	1.0×10^{-10}	2.39	2.2×10^{-11}	1.89
CH_2 + *hν* → CH + H	6.5×10^{-10}	1.89	3.3×10^{-10}	1.45	9.4×10^{-10}	1.42
CH_3 + *hν* → CH_2 + H	3.6×10^{-10}	2.06	2.0×10^{-10}	1.55	4.8×10^{-10}	1.54
CH_3 + *hν* → CH + H_2	3.6×10^{-10}	2.06	2.0×10^{-10}	1.55	4.8×10^{-10}	1.54
CH_3 + *hν* → CH_3^+ + e^-	3.3×10^{-10}	2.91	5.4×10^{-10}	2.23	8.1×10^{-12}	2.32
CH_4 + *hν* → CH_3 + H	4.7×10^{-10}	2.75	7.8×10^{-10}	2.22	5.3×10^{-11}	2.07
CH_4 + *hν* → CH_2 + H_2	8.8×10^{-10}	2.83	1.0×10^{-9}	2.23	7.0×10^{-11}	2.09
CH_4 + *hν* → CH + H_2 + H	1.2×10^{-10}	2.83	1.4×10^{-10}	2.23	9.7×10^{-12}	2.09
CH_4 + *hν* → CH_4^+ + e^-	1.4×10^{-11}	3.95	1.8×10^{-12}	3.36	1.4×10^{-13}	3.37
C_2 + *hν* → C + C	1.3×10^{-10}	2.97	3.9×10^{-11}	2.52	3.4×10^{-12}	2.45
C_2 + *hν* → C_2^+ + e^-	2.1×10^{-10}	3.82	3.9×10^{-11}	3.23	2.3×10^{-12}	3.22
C_2H + *hν* → C_2 + H	1.6×10^{-9}	2.48	1.8×10^{-9}	2.13	5.6×10^{-10}	1.83
C_2H_2 + *hν* → C_2H + H	4.4×10^{-9}	2.46	4.2×10^{-9}	2.08	1.9×10^{-9}	1.81
C_2H_2 + *hν* → $C_2H_2^+$ + e^-	3.3×10^{-10}	3.37	9.0×10^{-11}	2.87	6.0×10^{-12}	2.87
OH + *hν* → O + H	3.8×10^{-10}	2.33	5.1×10^{-10}	1.99	1.7×10^{-10}	1.62
OH + *hν* → OH^+ + e^-	5.2×10^{-12}	3.95	6.5×10^{-13}	3.35	5.5×10^{-14}	3.37
H_2O + *hν* → OH + H	6.8×10^{-10}	2.22	1.4×10^{-9}	2.01	3.4×10^{-10}	1.52
H_2O + *hν* → O + H_2	1.0×10^{-10}	2.70	3.5×10^{-10}	2.21	9.5×10^{-12}	1.74
H_2O + *hν* → H_2O^+ + e^-	2.7×10^{-11}	3.84	6.2×10^{-12}	3.22	3.6×10^{-13}	3.23
O_2 + *hν* → O + O	7.3×10^{-10}	2.31	3.5×10^{-10}	1.81	5.6×10^{-10}	1.77
O_2 + *hν* → O_2^+ + e^-	5.1×10^{-11}	3.72	1.2×10^{-11}	3.08	8.6×10^{-13}	3.08
H_2CO + *hν* → CO + H_2	1.6×10^{-9}	2.16	2.5×10^{-9}	1.80	1.0×10^{-9}	1.37
H_2CO + *hν* → H_2CO^+ + e^-	4.3×10^{-10}	3.22	1.0×10^{-10}	2.76	7.6×10^{-12}	2.69
CO_2 + *hν* → CO + O	1.1×10^{-9}	3.01	2.4×10^{-10}	2.41	4.3×10^{-11}	1.93
NH + *hν* → N + H	4.8×10^{-10}	2.46	2.0×10^{-10}	2.00	2.7×10^{-10}	1.94
NH + *hν* → NH^+ + e^-	1.8×10^{-12}	4.00	7.4×10^{-15}	3.41	1.7×10^{-14}	3.42
NH_2 + *hν* → NH + H	8.9×10^{-10}	1.92	4.2×10^{-10}	1.50	1.1×10^{-9}	1.47
NH_2 + *hν* → NH_2^+ + e^-	1.1×10^{-10}	3.44	3.1×10^{-11}	2.92	2.1×10^{-12}	2.91
NH_3 + *hν* → NH_2 + H	1.2×10^{-9}	1.99	6.9×10^{-10}	1.58	1.2×10^{-9}	1.41
NH_3 + *hν* → NH + H_2	3.1×10^{-10}	2.72	1.1×10^{-9}	2.21	3.6×10^{-11}	2.03
NH_3 + *hν* → NH_3^+ + e^-	4.2×10^{-10}	3.04	1.8×10^{-10}	2.34	8.2×10^{-12}	2.50
N_2 + *hν* → N + N	3.6×10^{-10}	3.81	7.6×10^{-11}	3.21	3.9×10^{-12}	3.19
CN + *hν* → C + N	1.0×10^{-9}	3.55	1.8×10^{-10}	3.02	1.2×10^{-11}	3.04
HCN + *hν* → CN + H	1.9×10^{-9}	2.82	4.5×10^{-9}	2.22	1.6×10^{-10}	2.01
HNC + *hν* → CN + H	9.4×10^{-10}	2.45	3.2×10^{-9}	2.16	3.9×10^{-10}	1.80
NO + *hν* → N + O	4.7×10^{-10}	2.01	2.3×10^{-10}	1.60	4.1×10^{-10}	1.41
NO + *hν* → NO^+ + e^-	2.6×10^{-10}	3.00	2.4×10^{-10}	2.27	8.7×10^{-12}	2.24
SH + *hν* → S + H	1.3×10^{-9}	1.89	2.0×10^{-9}	1.54	1.8×10^{-9}	1.30
SH^+ + *hν* → S + H^+	6.9×10^{-10}	1.89	3.2×10^{-10}	1.05	3.9×10^{-10}	0.80
H_2S + *hν* → SH + H	3.2×10^{-9}	2.26	3.4×10^{-9}	1.91	1.8×10^{-9}	1.58
H_2S + *hν* → H_2S^+ + e^-	7.2×10^{-10}	3.15	1.7×10^{-10}	2.68	1.3×10^{-11}	2.61
CS + *hν* → C + S	9.5×10^{-10}	2.60	4.2×10^{-9}	2.20	1.7×10^{-10}	1.98
CS + *hν* → CS^+ + e^-	1.7×10^{-10}	3.30	4.1×10^{-11}	2.81	2.8×10^{-12}	2.81
SO + *hν* → S + O	4.8×10^{-9}	2.24	1.1×10^{-8}	2.01	2.1×10^{-9}	1.47
SO + *hν* → SO^+ + e^-	2.1×10^{-10}	3.18	5.3×10^{-11}	2.72	4.0×10^{-12}	2.64
SO_2 + *hν* → SO + O	1.2×10^{-9}	2.25	2.1×10^{-9}	1.97	5.5×10^{-10}	1.47
SO_2 + *hν* → S + O_2	1.1×10^{-9}	2.29	2.1×10^{-9}	2.02	4.1×10^{-10}	1.47
SO_2 + *hν* → SO_2^+ + e^-	1.3×10^{-10}	3.77	3.0×10^{-11}	3.17	2.1×10^{-12}	3.16
HF + *hν* → H + F	1.3×10^{-10}	2.57	3.1×10^{-10}	2.18	2.7×10^{-11}	1.84
HCl + *hν* → H + Cl	2.0×10^{-9}	2.53	7.7×10^{-10}	1.99	4.2×10^{-10}	1.68
HCl + *hν* → HCl^+ + e^-	1.9×10^{-11}	3.91	2.7×10^{-12}	3.33	1.7×10^{-13}	3.35
C + *hν* → C^+ + e^-	3.3×10^{-10}	3.28	8.4×10^{-11}	2.82	5.8×10^{-12}	2.80
Si + *hν* → Si^+ + e^-	4.2×10^{-9}	2.49	4.4×10^{-9}	2.13	2.1×10^{-9}	1.91
P + *hν* → P^+ + e^-	1.1×10^{-9}	2.99	2.5×10^{-10}	2.48	2.3×10^{-11}	2.45
S + *hν* → S^+ + e^-	9.7×10^{-10}	3.09	2.1×10^{-10}	2.62	1.8×10^{-11}	2.55
Cl + *hν* → Cl^+ + e^-	4.7×10^{-11}	3.94	6.1×10^{-12}	3.35	4.4×10^{-13}	3.36
Na + *hν* → Na^+ + e^-	1.3×10^{-11}	2.12	1.6×10^{-11}	1.68	8.4×10^{-12}	1.47
Mg + *hν* → Mg^+ + e^-	6.7×10^{-11}	2.29	4.4×10^{-11}	1.80	5.4×10^{-11}	1.73
Fe + *hν* → Fe^+ + e^-	4.7×10^{-10}	2.45	6.9×10^{-10}	2.02	2.8×10^{-10}	1.88

[a] Interstellar radiation field (ISRF) of Draine (1978); see expressions in section 2.1.1.
[b] Radiation field of TW Hya scaled to the FUV energy density of the ISRF.
[c] Radiation field of AB Aurigae scaled to the FUV energy density of the ISRF.